Depinning in the quenched Kardar-Parisi-Zhang class I: Mappings, simulations and algorithm

Gauthier Mukerjee[1], Juan A. Bonachela[2], Miguel A. Muñoz[3], Kay Jörg Wiese[1]
[1] *Laboratoire de Physique de l'École Normale Supérieure, ENS, Université PSL, CNRS, Sorbonne Université, Université Paris-Diderot, Sorbonne Paris Cité, 24 rue Lhomond, 75005 Paris, France*
[2] *Department of Ecology, Evolution, and Natural Resources, Rutgers University, New Brunswick, NJ, United States*
[3] *Departamento de Electromagnetismo y Física de la Materia and Instituto Carlos I de Física Teórica y Computacional, Universidad de Granada, Granada, Spain*

Depinning of elastic systems advancing on disordered media can usually be described by the *quenched Edwards-Wilkinson* equation (qEW) which encompasses a broad universality class. However, additional ingredients such as anharmonicity and forces that cannot be derived from a potential energy may generate a different scaling behavior at depinning. An example of the latter is the Kardar-Parisi-Zhang (KPZ) term, proportional to the square of the slope at each site, which drives the critical behavior into the so-called *quenched KPZ* (qKPZ) universality class. Here, we show by using exact mappings supported by extensive numerical simulations that, at least for one- and two-dimensional interfaces, this class encompasses not only the qKPZ equation itself, but also anharmonic depinning and a well-known class of cellular automata introduced by Tang and Leschhorn. On the other hand, we cannot rule out the existence of distinct universality classes for $d > 2$. We then develop scaling arguments for all critical exponents. Dimension $d = 1$ is special since blocking configurations are directed-percolation (DP) clusters, allowing us to check scaling exponents against high-precision results from DP. To show that qKPZ is indeed the effective field theory for all these models, we develop an algorithm to measure the effective scale-dependent elasticity c, the effective KPZ non-linearity λ, and the effective disorder correlator $\Delta(w)$ across scales. This allows us to define the correlation length of the disorder $\rho := \Delta(0)/|\Delta'(0)|$, and a dimensionless universal KPZ amplitude $\mathcal{A} := \rho\lambda/c$, that takes the value $\mathcal{A} = 1.10(2)$ in all systems considered in $d = 1$. Using Graphical Processing Units, we are able to make further predictions in $d = 1$ and $d = 2$, and to some degree in $d = 3$. Our work paves the way for a deeper understanding of depinning transitions in the qKPZ class, and in particular, for the construction of a field theory that we describe in a companion paper.

I. INTRODUCTION

Diverse systems can be modeled as an elastic object (line, surface, manifold) advancing through a random medium with quenched disorder: disordered magnets and the associated Barkhaussen noise [1], expanding fronts of bacterial colonies [2, 3], systems that show self-organized criticality [4], or coffee imbibing this paper (if you are old fashioned enough to use a printout and to pour your coffee onto it) [5–7]. Often, the elastic system experiences a so-called "depinning transition" as a function of some driving parameter, so that the system changes from being pinned in some configuration to advancing at an average velocity [8]. This phase transition can be also thought of as the transition between an active state, where the elastic interface (or surface, etc) changes over time, and an absorbing or quiescent state, where the interface remains frozen [9]. At the transition, the dynamics becomes universal at sufficiently large scales, universality appears as microscopic details are irrelevant, and different systems and models can be grouped together into a few universality classes. The latter can then be studied via the renormalization-group (RG) and, more specifically, by employing functional renormalization group (FRG) approaches [10–16].

The simplest prototypical model for depinning transitions is the quenched Edwards Wilkinson equation (qEW), also called *harmonic depinning*. It monitors the height $u(x,t) \in \mathbb{R}$ of a d-dimensional interface embedded into $d+1$ dimensions. By construction, this excludes overhangs as well as bubbles. Its dynamics is described by

$$\eta\partial_t u(x,t) = \underbrace{c\nabla^2 u(x,t)}_{\text{harmonic elasticity}} + \underbrace{m^2[w-u(x,t)]}_{\text{driving force}} + \underbrace{F\big(x,u(x,t)\big)}_{\text{quenched disorder}}. \tag{1}$$

The disorder forces $F(x,u)$ are quenched Gaussian random variables with variance $\overline{F(x,u)F(x',u')} = \delta^d(x-x')\Delta_0(u-u')$. $\Delta_0(u)$ is the microscopic disorder-force correlator, assumed to decay rapidly for short-range (SR) disorder [8]. The system is driven by slowly increasing w, either as $w = vt$ (with v small), or via a small "kick", $w \to w + \delta w$ whenever the interface is stuck (pinned). The latter protocol is particularly useful to study avalanches [17–34].

While the microscopic force correlator $\Delta_0(u)$ can be analytic, the effective renormalized correlator $\Delta(w)$ seen in the field theory [10–16], and measurable in experiments [35–39] exhibits a cusp at $w = 0$. The slope at the cusp is proportional to the typical avalanche size, $|\Delta'(0^+)| \sim \langle S^2\rangle / \langle S\rangle$ [19].

The qEW class is not the only universality class for interface depinning. As we show here, there is one other rather large universality class, which we will establish is relevant whenever *non-linear effects cannot be neglected*. As an example, the coffee imbibing our paper can be modeled by the cellular automaton proposed in 1992 by Tang and Leschhorn (TL92) [40], or variants thereof [41, 42]. As it permeates through the paper, the coffee is blocked by a percolating line orthogonal to the coffee front, a phenomenon known as *directed-percolation depinning* (DPD) [5]. At a coarse-grained level one observes that the coffee front tends to grow in its normal direction, inducing anisotropy in the invaded medium. This phenomenon is modeled by an additional term,

usually called *KPZ term*, [43] in the equation of motion,

$$\eta\partial_t u(x,t) = ... + \underbrace{\lambda[\nabla u(x,t)]^2}_{\text{KPZ-term}}. \tag{2}$$

In addition to fluid invasion (our coffee front) [5–7], experiments on bacterial colonies [2, 3] or chemical reaction fronts [44, 45] share this property.

Finally, the elastic restoring force may be stronger than the harmonic elasticity in Eq. (1). This is particularly important at depinning in dimension $d = 1$, where the roughness exponent $\zeta = 5/4$ is larger than 1, meaning that the width of the interface grows stronger than the system size. As argued in Ref. [46] this implies that the small-displacement expansion for the elastic energy must be invalid, and one needs to go to the next order and include anharmonic elastic terms to bring the roughness to $\zeta \leq 1$.

We show below that all these models belong to the same universality class, termed the *quenched Kardar-Parisi-Zhang* (qKPZ) universality class [47]. The field theoretic treatment of qKPZ via FRG is, however, fraught with difficulties [48]. The reason is that in [48] the effective KPZ coupling λ generically flows to strong coupling, indicating that the perturbative treatment breaks down. Ref. [48] further contained a subspace of fixed points defined by closed RG equations. This subspace is characterized by an exponentially decaying effective disorder-force correlators $\Delta(w)$. Our study was motivated by the observation that such a fixed point is indeed realized for the pair-contact process (PCP) [49]. However, our numerical simulations indicate that none of the models discussed above has an exponentially decaying $\Delta(w)$. A new field theory that agrees with the simulations is therefore needed.

In view of the theoretical problems, here we tackle the system first numerically, and use the results to guide development of the theory. Apart from the effective disorder force correlator, $\Delta(w)$, we measured the flow of the parameters c and λ as a function of the confining potential strength m^2, to assess whether the effective non-linearity λ flows to infinity as in [48], or reaches a fixed point. The latter would allow us to *repair* the field theory. To answer these questions, we developed an algorithm to measure all effective parameters of our model. We conclude that an effective field theory with finite, m-dependent parameters exists, and has the form of the qKPZ equation. More specifically, we define a dimensionless effective KPZ amplitude $\mathcal{A}$,

$$\mathcal{A} := \frac{\lambda}{c}\rho, \tag{3}$$

where λ is the KPZ non-linearity in Eq. (2), c the effective elasticity in Eq. (1), and ρ the correlation length of the disorder in the driving direction, defined by $\rho := \frac{\Delta(0)}{|\Delta'(0^+)|}$. $\mathcal{A}$ should be viewed as the effective KPZ-nonlinearity in dimensionless units: It vanishes in qEW, and we show numerically that $\mathcal{A}$ is the same for TL92, qKPZ and anharmonic depinning. This supports our claim that there is only one universality class, which differs from qEW.

This paper is organised as follows: in Section II we describe in detail the models we use. We then show through mappings that such models are in the same universality class (section III). Section IV is devoted to a scaling analysis, with the confining potential m^2 defining a new class of exponents. How to measure the effective action is described in section V, starting with the disorder correlator (sections V B-V C), over the coupling constants (sections V E-V G). Brief conclusions are offered in section VI. In a companion paper [50] we show how to obtain the measured effective action from a field theory.

II. MODELS

In this section, we define three models. The first two are described by a continuous equation, while the third one is a cellular automaton model, i.e a discrete microscopic model. We show in section III that they can all be mapped onto each other.

A. QKPZ equation

The quenched KPZ equation (qKPZ) is defined as

$$\begin{aligned}\eta\partial_t u(x,t) = c\nabla^2 u(x,t) + \lambda\left[\nabla u(x,t)\right]^2 \\ +m^2\big[w - u(x,t)\big] + F\big(x, u(x,t)\big).\end{aligned} \tag{4}$$

Rescaling u, and $F(x,u)$, we could set $\lambda \to 1$. We prefer to not rescale the disorder, and thus λ will change under RG. Invariant under these transformations is the sign of λv, i.e. λ times the driving velocity $v = \mathrm{d}w/\mathrm{d}t$. A positive sign defines what is called the positive qKPZ equation. The negative qKPZ equation exhibits a very different phenomenology, with the propagating front spontaneously generating facets [44, 51, 52].

Discretization of the KPZ term (second term on the r.h.s. of Eq. (4)) is not trivial, and the choice made for it is important. We use the discretization of Ref. [53],

$$\begin{aligned}&u(x,t+\delta t) - u(x,t)\\ &= \delta t\Big\{m^2\Big[w - u(x,t)\Big] + F\big(x,u(x,t)\big)\\ &\quad + c\Big[u(x+1,t) + u(x-1,t) - 2u(x,t)\Big] +\\ &\quad + \lambda\left[\frac{u(x+1,t) - u(x-1,t)}{2}\right]^2\Big\}.\end{aligned} \tag{5}$$

$$\text{with } \lambda = 3, \quad c = 1, \quad \delta t = 0.01. \tag{6}$$

Our main control parameter m is varied between 0.05 and 0.6. The system size is chosen to be $L \leq 512$ with L the linear size. Following standard approaches, the disorder forces are drawn from a Gaussian distribution with unit variance, linearly interpolated between integer values of u. While efficient algorithms exists for the other two models, a direct simulation of the qKPZ equation is computationally expensive, and we have restricted our simulations to $d = 1$.

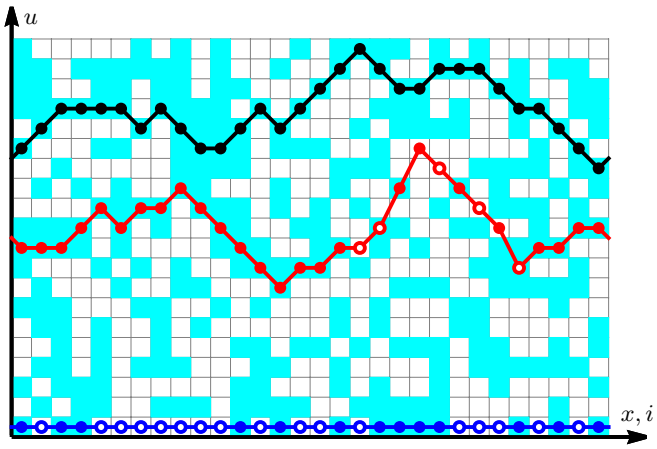

FIG. 1. The cellular automaton TL92. Blocking cells, i.e. cells above the threshold are drawn in cyan; those below in white. The initial configuration is the string at height 1 (dark blue). The interface moves up. An intermediate configuration is shown in red, the final configuration in black. Open circles represent unstable points, i.e. points which can move forward; closed circles are stable.

B. Anharmonic depinning

Anharmonic depinning (aDep) is defined by the equation

$$\eta\partial_t u(x,t) = \underbrace{c_4\nabla\cdot\Big\{\nabla u(x,t)\big[\nabla u(x,t)\big]^2\Big\}}_{\text{anharmonic elasticity}} + \underbrace{c\nabla^2 u(x,t)}_{\text{harmonic elasticity}} + \underbrace{m^2[w-u(x,t)]}_{\text{driving force}} + \underbrace{F\big(x,u(x,t)\big)}_{\text{quenched disorder}}. \tag{7}$$

If $\vec{\mathrm{e}}_i$ represents the unit vectors in d dimensions, the discretized anharmonic energies are

$$\mathcal{H}_{\mathrm{el}}[u] = \sum_x \sum_{i=1}^{d} \mathcal{E}_{\mathrm{el}}\big(u(x+\vec{\mathrm{e}}_i) - u(x)\big), \tag{8}$$

$$\mathcal{E}_{\mathrm{el}}(u) = \frac{c}{2}u^2 + \frac{c_4}{4}u^4. \tag{9}$$

The resulting elastic forces at site x are

$$-\frac{\delta\mathcal{H}_{\mathrm{el}}[u]}{\delta u(x)} = \sum_i \mathcal{E}'_{\mathrm{el}}\big(u(x+\vec{\mathrm{e}}_i)-u(x)\big) + \mathcal{E}'_{\mathrm{el}}\big(u(x-\vec{\mathrm{e}}_i)-u(x)\big)$$

$$= c\sum_{i=1}^{d}\Big[u(x+\vec{\mathrm{e}}_i) + u(x-\vec{\mathrm{e}}_i) - 2u(x)\Big] \tag{10}$$

$$+ c_4\sum_{i=1}^{d}\Big[u(x+\vec{\mathrm{e}}_i)-u(x)\Big]^3 + \Big[u(x-\vec{\mathrm{e}}_i) - u(x)\Big]^3.$$

The discretizations are similar to the qKPZ equation. For $d = 1$, we simulate systems with size up to $L = 2048$, assuming $m \le 0.05$. Using GPU in $d = 2$ allowed us to reach $L = 256$, with $m = 0.09$. In $d = 3$, we reached $L = 64$, and $m = 0.08$. To speed up simulations, we set $c = 0$, after checking that it gives the same results as $c = 1$. We varied the anharmonic term as $c_4 = 0.1, 0.2, 0.3$. There are 6×10^5 ($d = 1$), 5×10^4 ($d = 2$), and 2×10^4 ($d = 3$) independent samples. By construction, this system only moves forward, respecting the Middleton "no-passing" theorem [54], see section III A. This allows us to use the very efficient algorithm introduced in Ref. [55].

C. TL92

To describe fluid imbibition, Tang and Leschorn introduced the cellular automaton visualized in Fig. 1 (TL92) [40]. On a square lattice, each cell (i, j) is assigned a variable $f(i, j) \in [0, 1]$. If $f(i, j) < f_c$ the cell is considered closed (blocking). Otherwise the cell is considered open. The interface starts from a flat configuration at the bottom (dark blue on Fig. 1). A point $(i, j = u_i)$ on this interface is unstable and can move forward by 1, $u_i \to u_i + 1$, according to the following rules (in that order):

(i) links cannot be longer than 2. If a site is 2 cells ahead of its neighbors, stop.

(ii) if $f(i, j) > f_c$, move forward.

(iii) if one of the neighboring sites is 2 cells ahead, move forward.

While in the original version the critical force f_c is a constant [40], Here we choose it to depend on the height $j = u_i$ of the interface,

$$f_c := m^2[u_i - w]. \tag{11}$$

This has two consequences: first, as $f(i, j) \in [0, 1]$, rule (ii) is satisfied for all $u_i < w$, and never satisfied for $u_i > w+m^{-2}$. As a result, the interface is trapped in a domain of size m^{-2}. Increasing w, we can drive the interface as in qEW, Eq. (1). Our protocol is to keep w fixed until a stable configuration is reached, and only then increase w by δw. Two timescales are thus separated: a fast one governing the reorganization of the system, and an infinitely slower one corresponding to the driving. We use this protocol to calculate the effective disorder correlator and to simulate avalanches.

The interface is pinned when all its cells are blocking; its maximal slope is 1, see Fig. 1. This ensures that a directed-percolation path goes from left to right, i.e. perpendicular to the driving direction [40]. To be precise, the line gets pinned at the lowest percolating cluster (see Fig. 4 below). This relation to directed percolation allows us to use many of the high-precision results available for DP (see section IV B). Since time in the DP formulation is from left to right, whereas time for depinning of an interface is in the u direction, this correspondence is restricted to static quantities i.e. those corresponding to blocking configurations.

In our simulations of this cellular automaton, we use $L = 4096$ and $m \ge 0.02$ in $d = 1$. GPU computing allows us to reach $L = 256$ at $m = 0.05$ in $2d$, and $L = 128$ and $m = 0.1$ in $3d$.

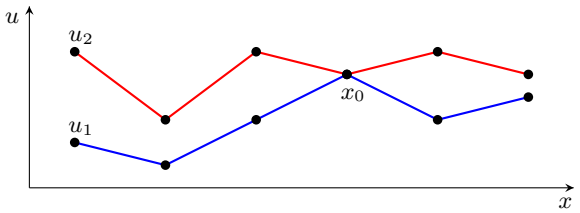

FIG. 2. Two configurations at depinning.

III. MAPPINGS

In this section we present different mappings between the three models introduced in sections II A to II C. Some of these mappings rely on no-passing theorems, which we prove below first.

A. No-passing theorems for TL92 and anharmonic depinning

In parallel to the famous no-passing theorem by Middleton [54] for harmonic depinning, we now prove a similar theorem for TL92 and anharmonic depinning.

1. *No-passing theorem for anharmonic depinning in the continuoum*

Assumptions.
• the elastic energy between nearest neighbors $\mathcal{E}(u)$ in Eq. (9) is a convex function,
• the disorder force $F(x,u)$ is continuous in u,
• $\dot{u}(x,t) \geq 0$.

No-Passing Theorem I (depinning in the continuuum).
• $\dot{u}(x,t') \geq 0$ for all $t' \geq t$.
• if two configurations are ordered, $u_2(x,t) \geq u_1(x,t)$, then they remain ordered for all times, i.e. $u_2(x,t') \geq u_1(x,t')$ for all $t' > t$.

Proof. Consider an interface discretized in x. The trajectories $u(x,t)$ are a function of time. Suppose that there exists x and $t' > t$ such that $\dot{u}(x,t') < 0$. Define t_0 as the first time when this happens, $t_0 := \inf_x \inf_{t'>t}\{\dot{u}(x,t') < 0\}$, and x_0 the corresponding position x. By continuity of F in u, the velocity $\dot{u}$ is continuous in time, and $\dot{u}(x_0,t_0) = 0$. This implies that the disorder force acting on x_0 does not change in the next (infinitesimal) time step, and the only changes in force can come from a change in the elastic terms. Since by assumption no other point has a negative velocity and the elastic energy $\mathcal{E}(u)$ is convex, this change in force can not be negative, contradicting the assumption.

To prove the second part of the theorem, consider the following configuration at time t_0: Here the red configuration is ahead of the blue one, except at position x_0, where they coincide. As in the first part of the proof, we wish to bring to a contradiction the hypothesis that at some later time $u_1(x_0)$ (blue in Fig. 2) is ahead of $u_2(x_0)$ (red). For this reason, we have chosen t_0 the infimum of times contradicting the theorem, $t_0 := \inf_{t'>t}\{u_1(x_0,t') > u_2(x_0,t')\}$. Consider the equation of motion for the difference between u_1 and u_2 at point x_0. According to Eqs. (7) and more generally (10),

$$\begin{aligned}\eta\partial_t \left[u_2(x_0,t) - u_1(x_0,t)\right]\big|_{t=t_0} \\ = \sum_{x=\mathrm{nn}(x_0,t_0)} \mathcal{E}'_{\mathrm{el}}\big(u_2(x,t_0) - u_2(x_0,t_0)\big) \\ -\mathcal{E}'_{\mathrm{el}}\big(u_1(x,t_0) - u_1(x_0,t_0)\big) \\ \geq 0. \end{aligned} \tag{12}$$

The sum runs over all nearest neighbours of x_0. The disorder forces have canceled as well as the term of order m^2, since by assumption $u_2(x_0,t_0) = u_1(x_0,t_0)$. The inequality follows from monotonicity of $\mathcal{E}'_{\mathrm{el}}(u)$, equivalent to the convexity of $\mathcal{E}(u)$.

2. *No-passing theorem for anharmonic depinning as a cellular automaton*

Assumptions.
• the positions $u(x,t)$ are integers; they can grow by 1 in an update, or remain constant.
• the elastic energy between nearest neighbors $\mathcal{E}(u)$ is convex.

No-Passing Theorem II (cellular automaton for depinning):
• if two configurations are ordered, $u_2(x,t) \geq u_1(x,t)$, then they remain ordered for all times, i.e. $u_2(x,t') \geq u_1(x,t')$ for all $t' > t$.

Proof. As for theorem I.

3. *No-passing theorem for TL92*

No-Passing Theorem III (TL92).
• if two configurations are ordered, $u_2(x,t) \geq u_1(x,t)$, then they remain ordered for all times, i.e. $u_2(x,t') \geq u_1(x,t')$ for all $t' > t$.

Proof. Consider again point x_0 on Fig. 2. By direct inspection of all possible configurations one shows that either nobody moves, red and blue move together, or only red moves. This works as well for parallel update as for single-site update, provided one updates both configurations at the same time.

B. Mapping from anharmonic depinning to TL92

1. *General idea*

The general idea is to show that, *for an appropriate choice of parameters*, both TL92 and anharmonic depinning have the same blocking configurations. This statement has two directions:
• a blocking configuration for TL92 is a blocking configuration for the depinning of an elastic line.
• all other configurations move forward.

We failed to prove the stronger statement, namely that each site stable in an allowed TL92 configuration is also stable for

depinning, and that only allowed TL92 configurations appear at depinning. This means that the dynamics of both models may be different, and even show different dynamical critical exponents.

2. *Cellular automaton in $d = 1$*

We aim to find the blocking configurations of TL92 with an interface whose law of evolution is the one of anharmonic depinning as given in Eq. (7), at least with a specific choice of parameters. To that end, we need to check for a given disorder that every configuration of the interface following the anharmonic depinning equation stops at the same configuration as in TL92. Let us start with a cellular automaton version. We choose disorder forces $F = \pm 1$, where $F = 1$ corresponds to open sites, and $F = -1$ to blocking sites. The height is integer, and whenever a site is unstable, it is moved ahead by 1, as in TL92. Whether a site moves or not depends only on its relative position to its nearest neighbors. Therefore, we only need to test whether there is agreement for 25 configurations: the two neighbors of a site can be separated by a distance with values in $\{-2, -1, 0, 1, 2\}$. The maximum distance is given by the TL92 rule that two neighbors can not be separated by a distance of more than 2, a condition anharmonic depinning needs to satisfy too. Symmetry of the forces under the exchange of the left and right neighbors decreases the number of distinct cases to 15. If one can find parameters c and c_4, such that the two prescriptions agree on those 15 configurations, the anharmonic depinning equation agrees for any interface configuration with TL92, and we have our mapping.

For each configuration to be tested, there are three sites to check: the left, the middle and the right ones. We note the relative position of the left and right neighbors: for example $(+1, +1)$ corresponds to a "v" shape with slope 1, $(-2, +2)$ to "/" with slope 2, and so on. Our considerations are for the middle point. If according to the TL92 rules it moves, the force felt by it must be ≥ 0, otherwise ≤ 0. The discretization of the equation of motion is given in Eq. (10), with elastic forces between two neighbors $c_4(u_i - u_{i+1})^3$. This gives the inequalities in Table I. With one exception, they are fulfilled by taking $c_4 \in]\frac{1}{7}, \frac{1}{2}[$; a centred value of $c_4 = 1/4$ is a good choice. Then in all cases anharmonic depinning has the same update rules as TL92, except for the configuration $(2, -2)$, a strongly inclined line. We did not succeed to tweak the model such that this configuration is also always stable at depinning. On the other hand, all blocking TL92 configurations are also blocking at depinning, and there is no configuration blocked at depinning which would move in TL92. Using the no-passing theorems II and III shows that both models have exactly the same blocking configurations, and that they are chosen independently from the history. Since anharmonic depinning can move faster than TL92, we conclude that their corresponding dynamical exponents should satisfy

$$z_{\mathrm{TL92}} \geq z_{\mathrm{aDep}}. \tag{13}$$

configuration	condition	configuration	condition
$(2, 2)$	$16c_4 > 1$	$(1, -2)$	$7c_4 > 1$
$(2, 1)$	$9c_4 > 1$	$(0, 0)$	true
$(2, 0)$	$8c_4 > 1$	$(0, -1)$	$-1 < c_4 < 1$
$(2, -1)$	$7c_4 > 1$	$(0, -2)$	$8c_4 > 1$
$(2, -2)$	false	$(-1, -1)$	$-1 < 2c_4 < 1$
$(1, 1)$	$-1 < 2c_4 < 1$	$(-1, -2)$	$9c_4 > 1$
$(1, 0)$	$-1 < c_4 < 1$	$(-2, -2)$	$16c_4 > 1$
$(1, -1)$	true		

TABLE I. Conditions on the anharmonic depinning coefficients, such that anharmonic depinning evolves as TL92, for each of the configurations in TL92.

3. *Cellular automaton in an arbitrary dimension*

We now generalize our considerations to an arbitrary dimension d. We first derive necessary conditions for a (globally) blocking configuration in TL92.

(i) A blocking configuration of TL92 has no site whose neighbor is at a distance -2.

(ii) A blocking configuration of TL92 has no site whose neighbor is at a distance 2.

As (ii) is trivial, we only need to prove (i): Suppose a site s_1 exists with a neighbor s_2 at a distance -2. Then their heights $u(s)$ satisfy

$$u(s_2) = u(s_1) - 2. \tag{14}$$

If site s_2 has a neighbor s_3 which is at a height distance -2, we continue to s_3, and so on. Since $u(s_i)$ is a decreasing sequence, and the minimum of all heights $u_{\min} := \min_s u(s)$ exists, this process stops, say at step n. By construction site s_n has no neighbor at distance -2, but at least neighbor s_{n-1} at distance 2. Thus site s_n is unstable, proving (i).

Let us now check for each site s its local configuration $l_s = (\delta u_1, ..., \delta u_{2d})$, defined as in section III B 2. We start with a globally blocking configuration in TL92. Due to (i) and (ii), all its $\delta u_i \in \{-1, 0, 1\}$. Whether the site is stable or not is *disorder decided*. We have to ensure that this is the same for anharmonic depinning. To simplify matters, we set $c \to 0$, only retaining c_4. In TL92 the site is unstable if $F = 1$ and stable if $F = -1$. Let us consider the stable case. In order to reproduce this in anharmonic depinning, we need that even if all neighbors pull in the opposite direction, i.e. are 1, the site remains stable. This implies the

(iii) condition from configuration $l_s = (1, 1, ..., 1)$:

$$c_4 < \frac{1}{2d}. \tag{15}$$

If the site in TL92 is unstable, the same condition arises, this time for the configuration $(-1, -1, ..., -1)$.

Next consider a configuration with one -2:

(iv) condition from $l_s = (-2, ...)$: none.

TL92 is blocked, while aDep may move or not. Due to the no-passing theorems, nothing has to be checked.

Remains to check a configuration with at least one 2:

(iv) condition from $l_s = (2, ...)$:

$$c_4(9 - 2d) > 1. \tag{16}$$

Proof: We need aDep to move. The worst case is that the disorder is $F = -1$, and that all remaining neighbors pull backwards. Since we have already excluded case (iv), they can maximally be at a distance -1. This gives the condition that the total elastic force $c_4[2^3 - (2d - 1)] > 1$. Simplifying yields Eq. (16).

We conclude that TL92 and aDep always find the same blocking configurations (in $d \leq 4$), as long as

$$\frac{1}{9 - 2d} < c_4 < \frac{1}{2d}. \tag{17}$$

This gives the bounds

$$\frac{1}{7} < c_4^{d=1} < \frac{1}{2}, \tag{18}$$

$$\frac{1}{5} < c_4^{d=2} < \frac{1}{4}. \tag{19}$$

In $d = 3$ there is no solution, but one can repeat the argument with an anharmonicity

$$\mathcal{E}_{\rm el}(u) = \frac{c_{2p}}{2p} u^{2p}. \tag{20}$$

While the bound (15) remains valid as a condition for c_{2p}, Eq. (16) changes to

$$c_{2p}(2^{2p-1} + 1 - 2d) > 1. \tag{21}$$

Therefore the simplest solution in $d = 3$ reads

$$\frac{1}{27} < c_6 < \frac{1}{6}. \tag{22}$$

This leaves open the possibility that in $d = 3$ several anharmonic-depinning universality classes exist. Both our simulations and the literature [5] are in favor of that hypothesis.

4. *Depinning in the continuum*

In [8] (section 5.7) a continuum model was proposed in $d = 1$ which finds the blocking configurations of TL92, and otherwise moves. The idea is to let the disorder act only close to integer values of u, and to provide a sufficiently strong force in between. This way anharmonic depinning stops at TL92 configurations, but never in between.

TL92 blocking			TL92 non-blocking		
configuration	condition		configuration	condition	
$(1,1)$	$c < \frac{1}{2}$	✓	(2,2)	$c > \frac{1}{4}$	✓
$(1,0)$	$c + \frac{\lambda}{4} < 1$	✓	$(2,1)$	$3c + \frac{\lambda}{4} > 1$	✓
$(1,-1)$	$\lambda < 1$	✓	$(2,0)$	$2c + \lambda > 1$	✓
$(0,0)$	true	✓	$(2,-1)$	$4c + 9\lambda > 4$	✓
$(0,-1)$	$-1 < c - \frac{\lambda}{4} < 1$	✓	$(2,-2)$	$1 + 4\lambda < 0$	
$(-1,-1)$	$c < \frac{1}{2}$	✓	$(1,-2)$	$4 + 9\lambda < 4c$	
			$(0,-2)$	$1 + \lambda < 2c$	
			$(-1,-2)$	$4 + \lambda < 12c$	✓
			$(-2,-2)$	$c > \frac{1}{4}$	✓

TABLE II. Set of conditions on the qKPZ coefficients for each possible configuration in TL92. $F = 1$ is the maximum disorder force. We can satisfy most conditions by choosing $c = 2/5$, $\lambda = 1/2$, as indicated by the checkmarks.

C. Mapping qKPZ to TL92

The mapping of qKPZ onto TL92 is more delicate as qKPZ has no no-passing theorem. On Fig. II we show the conditions to be satisfied for a cellular-automaton version of qKPZ, termed qKPZc. Inspection shows that not all conditions can be satisfied simultaneously. This remained true if we enlarged the space of allowed models. As an example, we allowed for an additional constant term in the equation of motion.

What we could however achieve, is that blocking configurations of TL92 are blocking for qKPZc, while most of the non-blocking configurations of TL92 are non-blocking for qKPZc, choosing

$$c = \frac{2}{5}, \quad \lambda = \frac{1}{2}. \tag{23}$$

The violating cases $(2,-2)$, $(1,-2)$ and $(0,-2)$ do not move in TL92, but move in qKPZc, bringing us out of the allowed configurations of TL92.

We now provide heuristic arguments that in the continuous version these configurations are not reached. In the continuum and close to the depinning transition, we have $\frac{\xi_\perp}{\xi_m} \to 0$. As a result, at large distances compared to the lattice cutoff but below the correlation length ξ_m, the interface must be flat on average. Now suppose that a series of sites are aligned and has the maximum slope α available. This extremal perturbation is shown in Fig. 3. We use the discretization of Eq. (6). We do not consider the disorder for simplicity. (It only enters in this argument through the structure of the space swept by the interface between avalanches.) If we name F_1 the force felt by the leftmost site of the slope, and F_N the force felt by the rightmost of the slope, then (independent of the KPZ term)

$$\Delta F_{1N} = F_N - F_1 = -2c\alpha. \tag{24}$$

As a result globally the perturbation gets flattened. For $i \in$

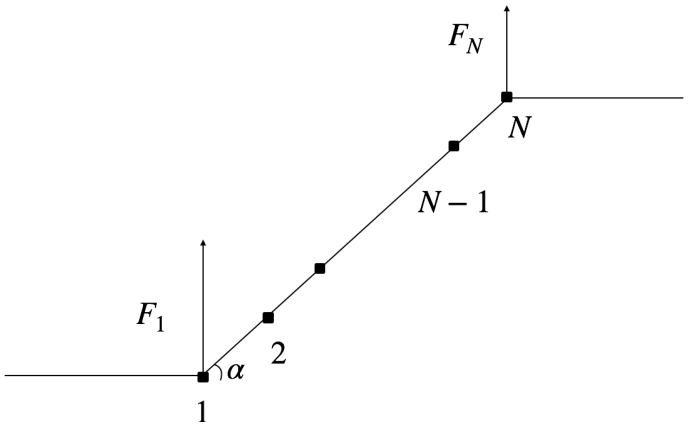

FIG. 3. Possible instability of the qKPZ equation, when a serie of locally aligned points have a slope α. The interface goes back to being flat at large distance, due to the $\xi_\perp/\xi_m \to 0$. The force felt by the lowest point is greater than the force felt by the lowest point. Below a certain slope α, this configuration do not generate a local slope above α.

$\{2, 3, ..., N-2\}$ we have $\Delta F_{i,i+1} = 0$. And finally

$$\Delta F_{12} = -\alpha c + \frac{3\lambda\alpha^2}{4}, \tag{25}$$

$$\Delta F_{N-1,N} = -\alpha c - \frac{3\lambda\alpha^2}{4}. \tag{26}$$

The local slope does not increase if $\alpha \leq \frac{4c}{3\lambda}$. With the previous values for λ and c this gives $\alpha \leq \frac{16}{15}$. So while we expect slope $\alpha = 1$ to be commonly reached, larger slopes are not. As a result, the configurations $(2, -2)$ and $(1, -2)$ are not reached, and that their associated conditions are not fulfilled does not matter. Finally, for the case $(-2, 0)$, it corresponds to the highest site of the perturbation. We can see from Eq. (26) that it always experiences a force that is weaker than the site just below, and as a result the local slope gets flattened and can not reach the value $(-2, 0)$. Adding disorder is statistically more likely to pin the site N, which feels a weaker forward force, than the site 1, accelerating the smoothening of the perturbation. We checked by numerical simulations of Eqs. (5)-(6) in $d = 1$, with forces set to $F = 1$ for an open cell, and $F = -1$ for a blocking cell, and $c = \frac{2}{5}$, $\lambda = \frac{1}{2}$ that qKPZ stops at the same blocking configuration as TL92.

D. Mapping anharmonic depinning to qKPZ

Starting from the anharmonic-depinning Eq. (7), the KPZ term is generated under renormalization, even in the limit of a vanishing driving velocity, $v \to 0^+$, which corresponds to depinning, under the combined action of the anharmonicity and the non analytic disorder force correlator. This was shown in [48], and is reproduced in the companion paper [50]. The KPZ term generated is then more *relevant*, in the renormalization-group sense, than the anharmonic elastic terms. This ensures that anharmonic depinning belongs to the qKPZ class.

$$\xi_\perp \sim \xi_\parallel^\zeta, \qquad \zeta = \tfrac{\nu_\perp}{\nu_\parallel}, \qquad \zeta_m = \tfrac{2\nu_\perp}{1+\nu_\perp},$$

$$\tfrac{\zeta_m}{\zeta} = \nu_\parallel(2-\zeta_m), \ \xi_m = Cm^{-\frac{\zeta_m}{\zeta}}, \qquad \beta = \tfrac{\zeta_m(z-\zeta)}{\zeta(2-\zeta_m)},$$

$$\Psi_\eta = z\tfrac{\zeta_m}{\zeta} - 2, \qquad \Psi_c = 2\tfrac{\zeta_m-\zeta}{\zeta}, \qquad \Psi_\lambda = 2\tfrac{\zeta_m-\zeta}{\zeta} - \zeta_m,$$

$$\tau = 2 - \tfrac{2}{d\frac{\zeta_m}{\zeta}+\zeta_m}, \ (1-\tau)\tfrac{d+\zeta}{z} = 1-\alpha.$$

TABLE III. All scaling relations derived in this paper. $\nu_\perp, \nu_\parallel$ come from DP mappings.

IV. CRITICAL EXPONENTS AND SCALING RELATIONS

Some scaling relations have already been derived [5, 40, 41], using the distance to the critical point as a control parameter. However, in order to construct the field theory, one has to introduce an infrared regularization acting in the x-direction. This is achieved by driving the surface using a confining potential with strength m^2, i.e. the term $m^2[w - u(x,t)]$ in Eqs. (1), (4), (7) and $m^2[u_i - w]$ in Eq. (11). It is this term which forbids rare large fluctuations in the u-direction. Moreover, this term is crucial for the field theory to have a fixed point [50], to measure the effective disorder forces (see section V below), and to quantitatively compare the RG flow between field theory and simulations. It is thus necessary to derive all scaling relations in terms of the *mass* m. As we show below, this introduces a new exponent ζ_m that gives the scaling of the field u in terms of m, instead of the usual scaling of u in terms of x. All relations are summarized in table III.

A. Definition of the 2-point function

The 2-point function is defined as

$$C(x-y) := \frac{1}{2}\overline{[u(x)-u(y)]^2} \sim \begin{cases} A|x-y|^{2\zeta}, & |x-y| \ll \xi_m \\ Bm^{-2\zeta_m}, & |x-y| \gg \xi_m \end{cases}. \tag{27}$$

The average is taken over disorder configurations. In contrast to qEW there appear two different exponents, ζ and ζ_m. While ζ is the standard roughness exponent, ζ_m describes how the plateau of the 2-point function scales with the strength m^2 of the confining potential. ξ_m marks the transition between the two asymptotic behaviours. It is the correlation length in the direction parallel to the interface, $\xi_\parallel = \xi_m$. Taking $x = \xi_m$ in the 2-point function, we get $A\xi_m^{2\zeta} \simeq Bm^{-2\zeta_m}$, and as a consequence

$$\xi_m = Cm^{-\frac{\zeta_m}{\zeta}}, \qquad C = \left(\frac{B}{A}\right)^{\frac{1}{2\zeta}}. \tag{28}$$

The correlation length perpendicular to the interface scales as $\xi_\perp \sim m^{-\zeta_m}$. In contrast to qEW $\zeta_m \neq \zeta$, and in particular

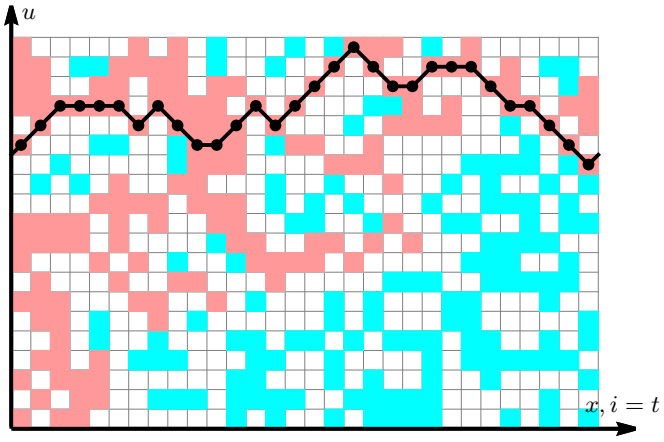

FIG. 4. Directed percolation from left to right. A site (i, u) is defined to be *connected* if it is occupied, and at least one of its left neighbors $(i-1, u)$, $(i-1, u \pm 1)$ is connected. The index i takes the role of time t.

$\xi_m \not\sim \frac{1}{m}$. A number of key features of this universality class stems from $\frac{\zeta_m}{\zeta} \neq 1$.

Before we show measurements (for TL92 in $d = 1$ in Fig. 5. Fig. 6, and for higher dimensions in Figs. 7-8), let us extract the critical exponents in $d = 1$ from directed percolation. This will serve as a strong check on our simulations.

B. Connection to directed percolation

In Sec. III we discussed that blocking configurations in TL92 are paths in directed percolation. Here we extract the exponents ζ and ζ_m from DP exponents. As the latter are known precisely [9, 56, 57], we get precise predictions for the former.

There are two guiding principles for these relations: all forces at depinning have the same scaling dimension, and every length parallel to the interface scales as x or ξ_m, while lengths in the perpendicular direction scale as $u \sim x^\zeta \sim m^{-\zeta_m}$.

Consider Fig. 4 which shows directed-percolation paths from left to right (in pink). They are constructed on a square lattice, where occupied cells (in pink or cyan) are selected with probability p, and the remaining once are unoccupied (white). A cell (i, j) is said to be connected to the left boundary (and colored pink) if it is occupied, and if at least one of its three neighbors $(i-1, j)$ and $(i-1, j \pm 1)$ is connected to the left boundary. The system is said to percolate if at least one point on the right boundary is connected to the left boundary. To achieve periodic boundary conditions for TL92, it is further required that this remains true for the periodically continued system.

While percolation is unlikely for small p, it is likely for large p, with a transition at $p = p_c$. There are three independent exponents β, $\nu_\parallel$, and $\nu_\perp$, defined via

$$\rho(t) := \left\langle \frac{1}{h} \sum_u s_u(t) \right\rangle \overset{t\to\infty}{\longrightarrow} \rho^{\text{stat}} \tag{29}$$

$$\rho_{\text{stat}} \sim (p - p_c)^\beta , \quad p > p_c, \tag{30}$$

$$\xi_\parallel = |p - p_c|^{-\nu_\parallel} , \tag{31}$$

$$\xi_\perp = |p - p_c|^{-\nu_\perp} . \tag{32}$$

Here $s_u(t)$ is the *activity* of site u at time t, set to one if the site is connected to the left boundary, and zero otherwise. $h = \sum_u$ is the height of the system, and ρ_{stat} the stationnary density of active sites. $\xi_\parallel$ is the size of the DP cluster along the parallel (time) direction, and $\xi_\perp$ the size in the transverse direction. The last two relations imply

$$\xi_\perp \sim \xi_\parallel^\zeta \implies \zeta^{d=1} = \frac{\nu_\perp}{\nu_\parallel} = 0.632613(3). \tag{33}$$

This is the roughness exponent ζ defined in Eq. (27). All numerical values are collected in table V.

For TL92, the surface is blocked by directed percolation paths in the direction parallel to the interface (from left to right). As a result, the distance to p_c in DP corresponds to a driving force in TL92 as $p - p_c = m^2(u - w)$. Together with $u \simeq \xi_\perp \sim (p - p_c)^{-\nu_\perp}$, this gives $m^2 \sim (p - p_c)^{1+\nu_\perp}$, or $(p - p_c) \sim m^{\frac{2}{1+\nu_\perp}}$. This finally yields

$$u \sim m^{-\zeta_m} \implies \zeta_m^{d=1} = \frac{2\nu_\perp}{1 + \nu_\perp} = 1.046190(4). \tag{34}$$

Note that in contrast to qEW $\zeta_m > \zeta$.

In $d \geq 2$ directed-percolation paths are 1-dimensional, whereas the interface is d-dimensional. As a result, the mapping breaks down and one has to introduce directed surfaces [58]. Since no information for our simulations is gained, we will not discuss this case.

C. Results for the 2-point function, ζ and ζ_m

For TL92 in $d = 1$, the 2-point function is shown on Fig. 5. $d = 2$ is covered in Figs. 6-7, while Fig. 8 is for dimension $d = 3$. The results for the critical exponents ζ and ζ_m are summarized in Table IV.

Let us first discuss our choice of simulation parameters. To obtain ζ, the smallest possible m is chosen, such that there is no system-spanning avalanche. The latter would mix the physics of the d-dimensional interface with that of a single degree of freedom. For ζ_m one needs a value of m that allows to clearly see the plateau of the 2-point function. Finally, we saw with seemingly little noise the 2-point function for larger systems, until $L = 1024$ for TL92, but we found systematic errors in those bigger systems, due to a lack of statistics. As a rule of thumb, 2×10^4 avalanches/per site are necessary to ensure a scaling collapse of the 2-point function for different sizes.

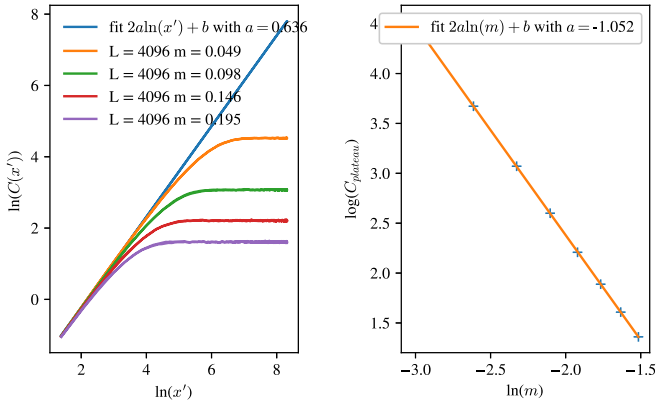

FIG. 5. TL92 $1d$ (left) 2-point function $C(x)$ for different values of m (not all shown here), plotted against $x' = \frac{4x(L-x)}{L}$ to take advantage of the periodic boundary conditions. We read off the exponent $\zeta = 0.636$ in the linear part of the curve (the slope is $2\zeta_k$). (right) Scaling of the plateau of the 2-point functions for different m. The fit yields $\zeta_m = 1.052$.

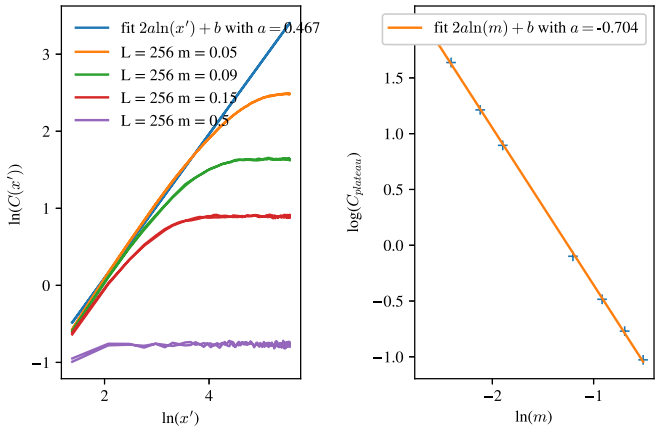

FIG. 6. TL92 $2d$ (left) 2-point function $C(x)$ along the diagonal of the system for different values of m (not all shown) plotted against $x' = \frac{4x\sqrt{2}(L\sqrt{2}-x\sqrt{2})}{\sqrt{2}L}$. The exponent $\zeta \approx 0.47$ is obtained from the linear part of the curve. (right) Scaling of the plateau of the 2-point functions for different m. The fit yields $\zeta_m = 0.70$.

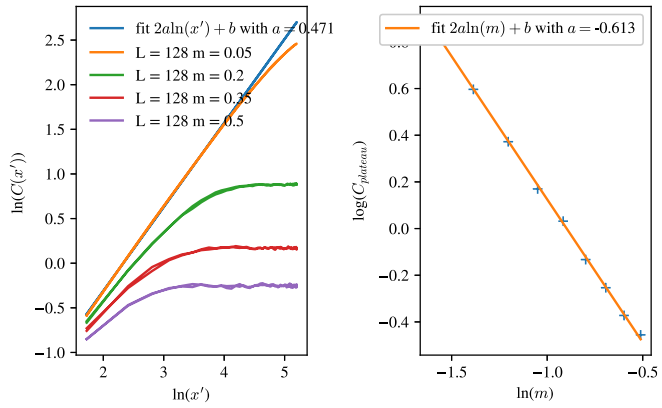

FIG. 7. Anharmonic depinning $2d$ (left) 2-point function $C(x)$ alongside the diagonal of the system for different values of m (not all shown here) plotted against $x' = \frac{4x\sqrt{2}(L\sqrt{2}-x\sqrt{2})}{\sqrt{2}L}$. The exponent $\zeta = 0.47$ is extracted from the linear part of the curve. (right) Scaling of the plateau of the 2-point functions for different m. The fit gives $\zeta_m = 0.61$.

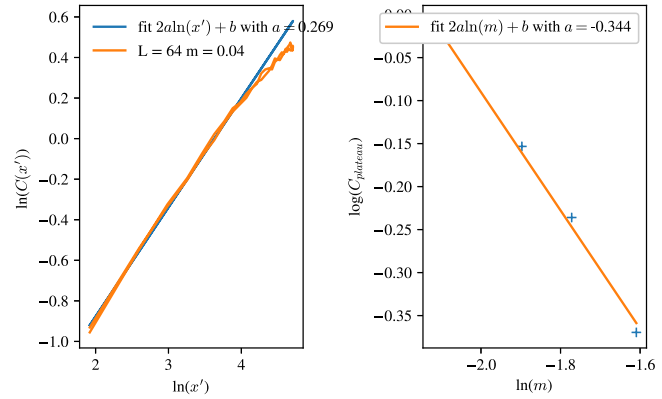

FIG. 8. Anharmonic depinning $3d$ (left) 2-point function $C(x)$ alongside the diagonal of the system for different values of m (not all shown) plotted against $x' = \frac{4x\sqrt{3}(L\sqrt{3}-x\sqrt{3})}{\sqrt{3}L}$. The exponent $\zeta = 0.27$ is read off from the linear part of the curve. (right) Scaling of the plateau of the 2-point functions for different m. The fit gives $\zeta_m = 0.34$.

Let us now discuss our results, summarized on tables IV and V. In $d = 1$, there are consistent values for ζ and ζ_m between the three simulated models, and directed percolation. We thus have confirmed numerically that there is a single universality class, and that the scaling arguments for ζ (known in the literature) and ζ_m (introduced here) are valid.

In $d = 2$, our simulations show that TL92 and anharmonic depinning share the same exponents. This is consistent with the mapping established in section III B 3.

In $d = 3$, the exponents seemingly differ, suggesting that the two universality classes may be different. This is consistent with the absence of a mapping established at the end of section III B 3. On the other hand, we cannot exclude that finite-size corrections, which are expected to be large for a cellular automaton such as TL92, are responsible for this lack of agreement.

D. The exponent ν

By definition of the correlation-length exponent $\nu_\parallel$, $\xi_m \sim (f - f_c)^{-\nu_\parallel}$, with f the driving force, and f_c the critical depinning force. This identifies the standard depinning exponent ν as

$$\nu^{d=1} = \nu_\parallel. \tag{35}$$

Since $(f-f_c) = m^2(u-w) \sim m^{2-\zeta_m}$, together with Eq. (28) this implies

$$\frac{\zeta_m}{\zeta} = \nu(2-\zeta_m). \tag{36}$$

model	ζ	ζ_m	ζ litterature
aDep 1d	0.635(6)	1.054(3)	0.63 [46]
TL92 1d	0.636(8)	1.052(5)	0.63 [5]
qKPZ 1d	0.64(2)	1.05(1)	0.633(8) [53]
qEW 1d	1.25(1)	1.25(1)	1.25 [46, 59, 60]
aDep 2d	0.48(2)	0.61(2)	0.45(1)[46]
TL92 2d	0.47(3)	0.70(3)	0.48(3) [5]
qEW 2d	-	-	0.753(2) [46]
TL92 3d	0.44(5)	0.52(6)	0.38(4) [5]
aDep 3d	0.27(4)	0.34(4)	0.25(2) [46]
qEW 3d	-	-	0.355(1) [46]

TABLE IV. Critical exponents ζ and ζ_m of the qEW and qKPZ classes, from simulations of anharmonic depinning and comparison with the literature.

exponent	DP value	measured value
$\nu_\parallel$	1.733847(6),	
$\nu_\perp$	1.096854(4),	
ζ	0.632613(3),	0.636(4)
ζ_m	1.046190(4),	1.052(6)
$\frac{\zeta_m}{\zeta}$	1.65376(1),	1.65(1)
τ	1.259246(3),	1.257(5)
ψ_c	1.30752(2),	1.31(4)
ψ_λ	0.26133(2),	0.28(3)
z	-	1.10(2)
α	-	1.28(3)
ψ_η	-	$-0.18(1)$
β	-	0.81(3)

TABLE V. The DP values for all exponents are from Ref. [9] (first two lines), combined with the scaling relations derived here (following lines). The agreement between the static exponents measured for aDep and TL92 and their DP values is excellent. There is no such mapping for dynamical exponents. The conjecture $z = 1$ advanced in Ref. [5] is in contradiction to our simulations, see Appendix A for a detailed discussion.

This relation is valid in any dimension $d \leq d_c$ and does not rely on the mapping to DP. In $d = 1$ replacing ζ_m and ζ by their expressions in terms of $\nu_\perp$ and $\nu_\parallel$ given in Sec. IV B, we verify consistency.

E. Dynamical exponent z

For the velocity of an avalanche by definition $v \sim (f-f_c)^\beta$, and $v = \frac{u}{t} = \frac{\xi_\perp}{\xi_\parallel^z} = \xi_\parallel^{\zeta - z} = (f - f_c)^{-\nu_\parallel(\zeta - z)}$. Eliminating

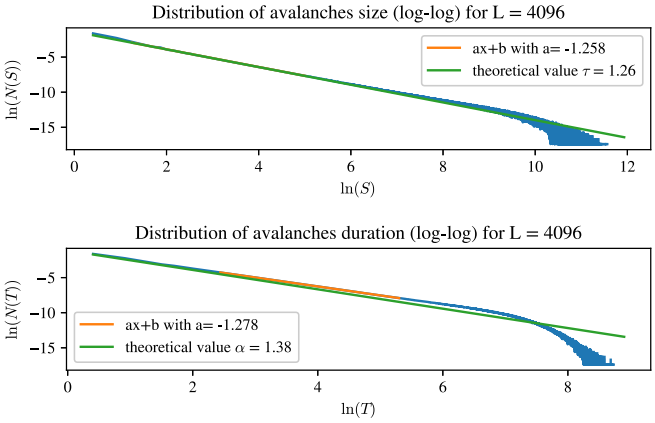

FIG. 9. Avalanches-size and duration distributions for TL92. τ and α are the associated exponents. We also computed S_m and T_m from these distributions at different m and verified the relations Eq. (43) and Eq. (47) (not shown).

$\nu_\parallel$ with the help of Eq. (36) we get

$$\beta = \frac{\zeta_m(z-\zeta)}{\zeta(2-\zeta_m)}. \tag{37}$$

Scaling relations for qEW are recovered by setting $\zeta_m = \zeta$, resulting in

$$\beta_{\text{qEW}} = \frac{z-\zeta}{2-\zeta} = \nu(z-\zeta). \tag{38}$$

We measured z in TL92 in $d = 1$ by looking at the joint distribution of avalanche duration T and lateral extension ℓ, shown in Fig. 10 (see section IV G for details). Using

$$T \sim \ell^z, \tag{39}$$

we find

$$z_{\text{TL92}}^{d=1} = 1.10 \pm 0.02. \tag{40}$$

This value contradicts Ref. [5], which conjectures the *exact* value $z = 1$ using heuristic arguments and evidence from numerical simulations. Our simulation, like theirs, computes the lateral extension of an avalanche as a function of its duration. While Ref. [5] extracts the power law by a fit to one decade, we have data on more than 2.5 decades, allowing for a much more precise value. We reviewed the argument given in Ref. [5], which relies on shortest paths on a percolation cluster. Our main criticism is that transport properties on percolation clusters are linked to the proportion of singly-connected bonds, bonds that if cut, separate the percolation cluster into two parts, (the "blobs and links" representation [61]). Even if the perpendicular direction is small compared to the longitudinal one, it is non zero, which changes the proportion of singly connected bonds. More details are given Appendix A.

F. Avalanche size

Let us recall scaling for avalanches, adapted to the qKPZ case. Let S the size of an avalanche, i.e. is the number of sites

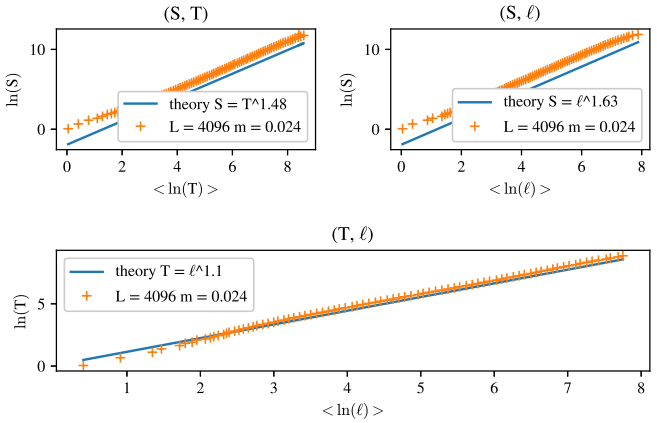

FIG. 10. Joint distributions of (S,T), (S,ℓ), (T,ℓ) in TL92, in $d=1$. They verify Eqs. (46), (42) and the definition of z in Eq. (39). Averaging before or after taking the log gives similar results.

that are affected in an avalanche (in a cellular automaton), or the volume swept through by the interface between two blocking configurations. Define its typical size S_m as

$$S_m := \frac{\langle S^2\rangle}{2\langle S\rangle}. \tag{41}$$

Scaling implies that

$$S \sim \ell^{d+\zeta} \quad \Longrightarrow \quad S_m \sim \xi_m^{d+\zeta}, \tag{42}$$

where ℓ is the lateral extension of an avalanche. Injecting Eq. (28) yields

$$S_m \sim m^{-d\frac{\zeta_m}{\zeta}-\zeta_m}. \tag{43}$$

Assume that $P_S(S) \sim S^{-\tau}$ for $S \ll S_m$. To obtain a scaling relation for τ, follow [27] to consider the avalanche-size distribution per unit force,

$$\rho_f(S) := \frac{\delta N(S)}{\delta f} \simeq S^{-\tau} f_S\left(S/S_m\right) g_S\left(S/S_0\right), \quad S_0 \ll S_m. \tag{44}$$

S_m is the large-scale cutoff introduced above, while S_0 is a small-scale cutoff. We expect Eq. (44) to have a finite limit when $m \to 0$ [27]. Associated to a force increase by δf is a total displacement $\int_x \delta u(x) = \langle S\rangle$. The total increase in force can be written as $\delta f = \int_x m^2 \delta u(x) = m^2\langle S\rangle$. By the definition of ρ_f we have $\langle S\rangle = \delta f \int_0^\infty S\rho_f(S)\mathrm{d}S$. This gives

$$1 = m^2\left[S_m^{2-\tau} - \mathcal{O}(S_0^{2-\tau})\right].$$

Since $\tau < 2$, we can take the limit of $S_0 \to 0$, resulting in

$$\tau = 2 - \frac{2}{d\frac{\zeta_m}{\zeta}+\zeta_m}. \tag{45}$$

We compare this result to simulations in section IV H below.

G. Avalanche duration

Consider the dynamics of an avalanche, with ℓ its lateral extension and T its duration. Using $T \sim \ell^z$ and $S \sim \ell^{d+\zeta}$, we get

$$S \sim T^{\frac{d+\zeta}{z}}. \tag{46}$$

Assume that

$$P_T(T) \sim T^{-\alpha} \quad \text{for } T \ll T_m := \frac{\langle T^2\rangle}{2\langle T\rangle}. \tag{47}$$

Scaling implies that $P_S(S)\mathrm{d}S \sim P_T(T)\mathrm{d}T$. For small avalanches (but bigger than the discretization cutoff) this implies that $S^{1-\tau} \sim T^{1-\alpha}$. Using Eq. (46) we obtain

$$\alpha = 1 + \frac{1}{z}\left(d+\zeta - \frac{2\zeta}{\zeta_m}\right). \tag{48}$$

H. Numerical simulations for size and duration

Let us first explain our choice of parameters: to study avalanches, it is important to avoid triggering two overlapping avalanches; to that end, we use a driving strength $w \to w+\delta w$ such that the probability that a site gets depinned is $\frac{1}{40}$. As a comparison, in the other simulations we generate on average one avalanche per driving event. Next, m should be large enough to avoid system-spanning avalanches. For $L = 4096$ we computed our distributions for 2×10^7 avalanches and $m = 0.0244$.

We verified the scaling relations for the dynamic exponent z and the size and duration exponents τ and α. To this end, we recorded for TL92 in $d=1$ the joint distribution of (S,T,ℓ), with ℓ the lateral extension of the avalanche. This allowed us to extract three joint distributions involving two variables, and shown on Fig. 10. First, we use $T \sim \ell^z$ to extract z in $d=1$ as

$$z^{d=1} = 1.10(2). \tag{49}$$

This gives for the remaining relations the numerical values $T \sim \ell^{1.48(3)}$, and $S \sim \ell^{1.6326(3)}$. A glance on Fig. 10 shows that the data are in good agreement with these values.

Fig. 9 shows the size and duration distributions, with predicted exponents $\tau = 1.2592(6)$, and $\alpha = 1.385(7)$. While the former is satisfied over almost three decades, the latter seemingly comes out much smaller, namely at

$$\alpha_{\mathrm{TL92}}^{d=1} = 1.28(2) \tag{50}$$

Let us discuss possible sources for this discrepancy:
(i) The real functional form of P_T is more complicated than the scaling anzatz in Eq. (47), and has a "shoulder" that pushes the apparent exponent down. This phenomenon was described for the size distribution P_S in qEW, both numerically [18] and within the FRG [19]; it was studied numerically for P_S on qKPZ [62]. As the top plot of Fig. 9 shows, there is a small

shoulder for P_S, but the agreement on the exponent is very good. If the shoulder for P_T is much longer, it is hard to see on Fig. 9.
(ii) We still see large finite-size corrections due to the discretization of the time evolution. This would be surprising in view of the excellent scaling in the (T, ℓ) and (S, T) plots of Fig. 10.

We could properly simulate avalanche durations only in a cellular automaton, since for anharmonic depinning we used the variant Monte Carlo algorithm of [46, 63], which has a different (probably faster) time evolution. Whether this amounts to a smaller exponent z is however doubtful.

V. EFFECTIVE DISORDER $\Delta(w)$ AND RUNNING COUPLING CONSTANTS

A. Definition of the effective disorder $\Delta(w)$

In Eqs. (1), (4) and (7) we had introduced a restoring force $m^2[w-u(x,t)]$ from a confining potential. This was not only necessary to drive the system, but also to measure the effective force correlator $\Delta(w)$, by measuring the fluctuations of the center-of-mass position u_w of the interface. Define $\Delta(w)$ as

$$\Delta(w-w') := m^4 L^d \overline{(u_w - w)(u_{w'} - w')}^{\rm c}, \tag{51}$$

$$u_w := \frac{1}{L^d}\int_x u_w(x), \tag{52}$$

$$u_w(x) := \lim_{t\to\infty} u(x,t) \text{ given } w \text{ fixed}. \tag{53}$$

In this protocol, w is increased in steps. One then waits until the interface stops, which defines $u_w(x)$. Its center-of-mass position is u_w, and its fluctuations define $\Delta(w)$.

B. Scaling of $\Delta(w)$

The definition (51) has a finite limit for fixed m, when $L \to \infty$. Using that $u \sim m^{-\zeta_m}$, and that L/ξ_m is dimensionless leads together with Eq. (28) to

$$\Delta(0) \sim m^{4-d\frac{\zeta_m}{\zeta}-2\zeta_m}. \tag{54}$$

For the argument of $\Delta(w)$, we expect

$$w \sim u \sim m^{-\zeta_m}. \tag{55}$$

A non-trivial check is as follows: As in qEW, one can connect the typical avalanche size given in Eq. (41) to the disorder force correlator (see e.g. [8], Eq. (104)),

$$|\Delta'(0^+)| = m^4 \frac{\langle S^2\rangle}{2\langle S\rangle} \sim m^{4-\zeta_m(d/\zeta+1)}. \tag{56}$$

This is consistent with Eqs. (54) and (55).

C. Measuring $\Delta(w)$

$\Delta(w)$ is defined from the variable u_w in Eq. (53). For depinning, be it anharmonic or not, integrating the equation of motion with periodic boundary conditions leads to

$$m^2(u_w - w) = F_w, \tag{57}$$

$$F_w := \frac{1}{L^d}\int_x F(x, u_w(x)). \tag{58}$$

Thus $\Delta(w)$ is also the correlator of the disorder acting on the interface. This direct connection breaks down in qKPZ, as after integration over the center of mass three terms remain: $m^2(w-u_w)$, F_w, and Λ_w, defined by

$$\Lambda_w := \frac{1}{L^d}\int_x \lambda[\nabla u_w(x)]^2. \tag{59}$$

A configuration at rest then has

$$m^2(w-u_w) + F_w + \Lambda_w = 0. \tag{60}$$

We note that while the first and last term are positive, the middle term is negative. So why did we define $\Delta(w)$ as the (connected) correlations of u_w, and not F_w? After all, we call it the *renormalized force correlator*. The answer comes from more sophisticated field theory arguments, developed in a companion paper [50]. In essence it looks at all 2-time contributions to the uu correlations, and then amputates the external response functions. The result is as given in Eq. (51). For details we refer to [50].

We have verified that Eqs. (54)-(56) hold for TL92, and the other two models. The correct regime to obtain a good scaling collapse for the correlator – with the exponents given in Table IV – is when the infrared cutoff is set by the confining parabola, meaning that the plateau of the 2-point function is reached. The results for the shape of $\Delta(w)$ are summarized in Figs. 11 and 12, where everything is rescaled such that $|\Delta'(0^+)| = \Delta(0) = 1$.

D. Anomalous dimensions for c, λ, and η

If there were no corrections to c, λ and η, the theory would be trivial. Before we show in the next section V E an algorithm to measure their scale dependence, let us first derive their anomalous dimensions, given the information already obtained.

Let us define their scaling dimensions as

$$\lambda \sim m^{-\psi_\lambda} \tag{61}$$

$$c \sim m^{-\psi_c} \tag{62}$$

$$\eta \sim m^{-\psi_\eta}. \tag{63}$$

Equating the dimensions of driving force and elasticity, $c\nabla^2 u \sim m^2 u$, we get $m^{-\psi_c-\zeta_m}\xi_m^{-2} \sim m^{2-\zeta_m}$ and together with Eq. (28)

$$\psi_c = 2\frac{\zeta_m - \zeta}{\zeta}. \tag{64}$$

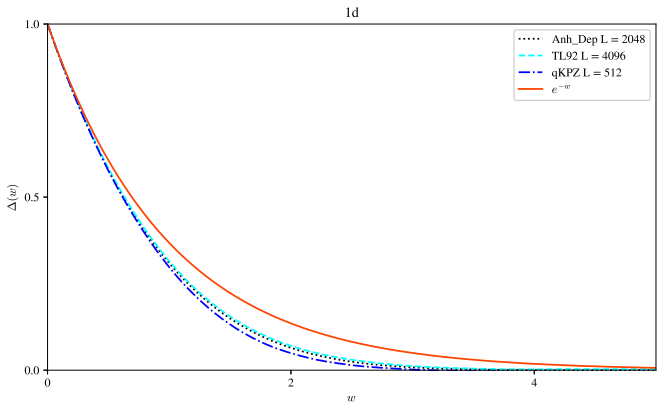

FIG. 11. Comparison of the shapes of the correlators in $d = 1$ and for anharmonic depinning, TL92 and qKPZ with the exponential behavior observed in a subspace in Ref. [48]. We clearly see (a): The correlators for TL92, aDep and qKPZ are very close. (b) The subspace found in [48] is not the one attained by the evolution of those models. The shapes have been normalized by setting $|\Delta'(0^+)| = \Delta(0) = 1$.

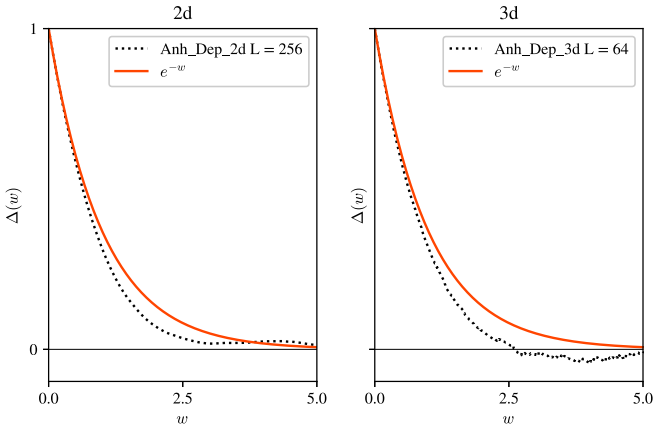

FIG. 12. Comparison of the shapes of the correlators in $d = 2, 3$ for anharmonic depinning with the exponential behavior found for a subspace in Ref. [48]. We see that this subspace is not the one attained by these models. The shapes are normalized s.t. $|\Delta'(0^+)| = \Delta(0) = 1$.

A similar argument for λ yields

$$\psi_\lambda = 2\frac{\zeta_m - \zeta}{\zeta} - \zeta_m. \tag{65}$$

These two relations have been verified (see left of Fig. 15), thanks to the algorithm we describe in Sec. V E.

The scaling relation for ψ_η is obtained from $\eta\partial_t u \sim m^2 u$, implying $t \sim m^{-2-\psi_\eta} \sim x^{(2+\psi_\eta)\zeta/\zeta_m}$. This yields

$$\psi_\eta = z\frac{\zeta_m}{\zeta} - 2. \tag{66}$$

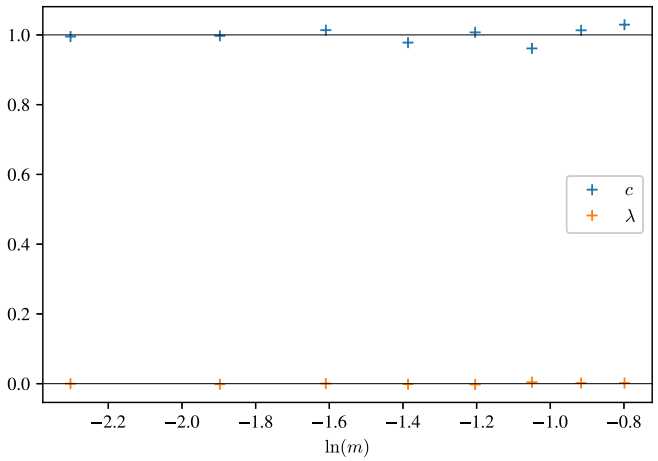

FIG. 13. The measured effective c and λ for the qEW equation. The effective elasticity c is unrenormalized (with noticeable simulation errors at large m), as predicted by the statistical tilt symmetry (STS). The measured non-linearity λ vanishes.

E. An algorithm to measure the effective coupling constants

In order to obtain the effective KPZ non-linearity λ, one can tilt the system and measure the change in the depinning force as in [47]. In contrast, the effective elasticity c has to our best knowledge never been measured. Since the field theory in Ref. [48] did not deliver an FRG fixed point for the ratio λ/c, we decided to check numerically whether such a fixed point exists, and to extract as much information as possible to constrain the field theory.

Our algorithm to achieve this is simple: measure the response of the interface to a perturbation, sinusoidal in space, and constant in time. This is achieved by driving the system with a spatially modulated background field $w(x)$, see Fig. 14,

$$w(x) = w_0 + A\sin\left(f\frac{2\pi x}{L}\right). \tag{67}$$

After each avalanche, we increase $w(x)$ by δw (a constant), $w(x) \to w(x) + \delta w$. We focus on the slowest mode $f = 1$. We then measure the mean interface profile, i.e. its *response*, $\overline{u(x)}$. Varying the amplitude A of the driving, we fit this response with a polynomial in A. The effective parameters are then linked to the projections on these modes. To be specific, write, with $\ell := L/2\pi$,

$$\overline{u(x)} = u_0(A) + u_1(A)\sin\left(\frac{x}{\ell}\right) + u_2(A)\cos\left(\frac{2x}{\ell}\right) + ... \tag{68}$$

$$u_0(A) = {}^0u_0 + {}^2u_0A^2 + \mathcal{O}(A^4), \tag{69}$$

$$u_1(A) = {}^1u_1A + \mathcal{O}(A^3), \tag{70}$$

$$u_2(A) = {}^2u_2A^2 + \mathcal{O}(A^4). \tag{71}$$

The dots represent higher-order terms in A, while the double-indexed u's are numbers to be measured. The lower index represents the mode, while the upper index is the order in A.

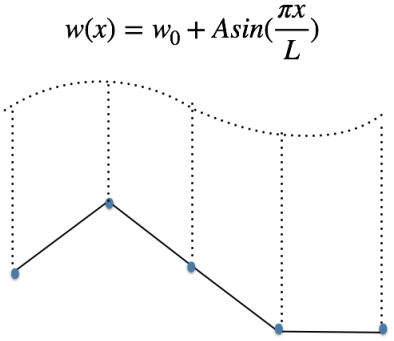

FIG. 14. We drive the interface with a spatially modulated driving. The continuous black line is the interface with blue dots representing sites

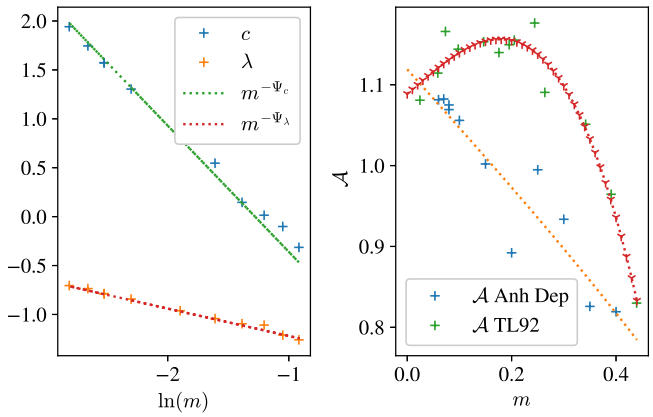

FIG. 15. Left: Scaling of c and λ for anharmonic depinning in 1d. Right: Measured amplitude ratios $\mathcal{A}$ for TL92 and anharmonic depinning. The second-order polynomial fits show convergence to $\mathcal{A} \approx 1.10(2)$ for $m \to 0$.

We inject this development into the noiseless KPZ equation

$$-m^2 u + c\nabla^2 u + \lambda(\nabla u)^2 = -m^2 A \sin\left(\frac{x}{\ell}\right). \tag{72}$$

It is the non-linear term in this equation that generates the higher harmonics. The parity of the number of derivatives restricts the allowed modes to those in Eq. (68). Matching coefficients, we find

$$^0u_0 = w_0 \tag{73}$$

$$^1u_1 = \frac{m^2}{m^2 + \frac{c}{\ell^2}}, \tag{74}$$

$$^2u_0 = \frac{m^2\lambda}{4\ell^2(m^2 + \frac{c}{\ell^2})^2}, \tag{75}$$

$$^2u_2 = \frac{m^4\lambda}{4\ell^2(m^2 + \frac{4c}{\ell^2})(m^2 + \frac{c}{\ell^2})^2}. \tag{76}$$

These relations are inverted to obtain λ and c,

$$c(m) = m^2\ell^2 \frac{1 - {}^1u_1}{{}^1u_1}, \tag{77}$$

$$\lambda(m) = 4m^2\ell^2 \frac{{}^2u_0}{({}^1u_1)^2}. \tag{78}$$

F. Tests and results

Let us start with some tests of our procedure for qEW. There $\lambda(m) \equiv 0$, and there is no renormalization of c, as it is protected by the statistical-tilt symmetry, the statistical invariance of the equation of motion under the transformation $u(x,t) \to u(x,t) + \alpha x$. In Fig. 13 we show simulations for harmonic depinning (Eq. (7) with $c_4 = 0$ and $c_2 = 1$). We measured the effective elastic constant c, and see that it does not renormalize and stays at $c = 1$. Moreover, the measured $\lambda = 0$.

We next apply our procedure to TL92 and anharmonic depinning in $d = 1$, see Fig. 15. For each m, the polynomials were fitted on 100 different values for A, and each value of A corresponds to a simulation of 10^5 independent samples. The size varies from $L = 512$ to $L = 2048$, since for larger values of m smaller systems are sufficient. We find

$$\psi_c^{d=1} = 1.31 \pm 0.04, \tag{79}$$

$$\psi_\lambda^{d=1} = 0.28 \pm 0.03, \tag{80}$$

in agreement with their expressions in Eqs. (64)-(65), and the numerical values given in table V.

We checked that higher-order relations (given in Appendix B) give the same values for c and λ. We further checked that the results given for λ are the same as those obtained as a response to a tilt. (Note that to introduce a tilt with our driving protocol, one has to tilt both the driving potential and the interface.)

The determination of the effective parameters λ and c is not the only application of this algorithm: one can measure the effective decay of subleading parameters present in the microscopic model, such as c_4, and obtain valuable information on the crossover to the qKPZ universality class. This may be helpful for experiments and is summarized in Appendix B. While many things can be measured, this technique is limited by the available computer resources, as illustrated on Fig. 18 for the decay of c_4.

G. The universal KPZ amplitude $\mathcal{A}$

An important question is whether qKPZ is the proper large-distance description of TL92, anharmonic depinning, and itself (i.e. a numerical implementation of the qKPZ equation). To ensure this, the properly renormalized non-linearity λ needs to flow to a fixed point. While λ and c both flow, i.e. do not go to a fixed point by themselves, this is achieved by defining the *universal KPZ amplitude* $\mathcal{A}$, defined as

$$\mathcal{A} := \frac{\Delta(0)}{|\Delta'(0^+)|}\frac{\lambda}{c}. \tag{81}$$

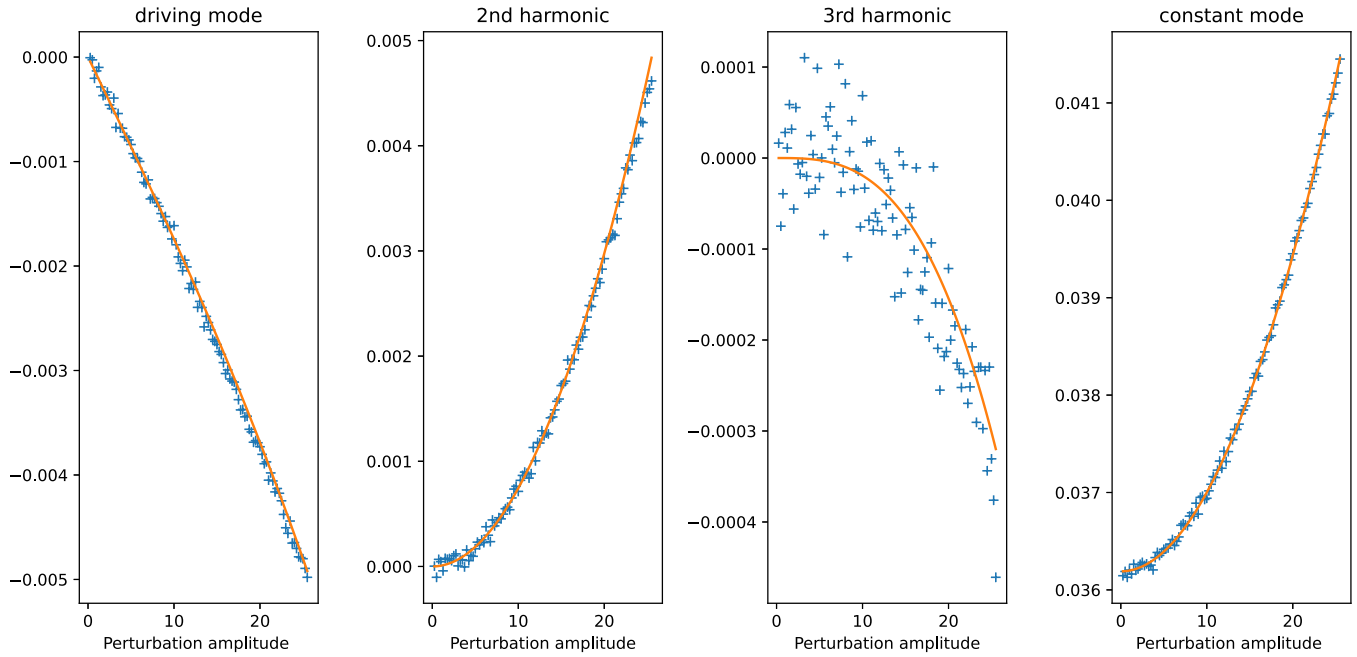

FIG. 16. Measuring the modes of the interface for different driving amplitude A. From the orange fits we get the different numbers ${}^{i}u_j$ defined. For example from the fit of the driving mode we get ${}^{1}u_1$ and ${}^{3}u_1$. The polynomial behaviour predicted in Eq. (71) is verified. The shown plots are for anharmonic depinning, $L = 1024$, and $m = 0.06$. The perturbation amplitude is in lattice units.

The idea behind this construction is that if both λ and c are relevant, then

$$\lambda \left[\nabla u(x,t)\right]^2 \sim c\nabla^2 u(x,t) \quad \Longrightarrow \quad \frac{\lambda}{c} \sim \frac{1}{u} \tag{82}$$

On the other hand $\Delta(u) \sim u\Delta'(u)$, thus we can define a correlation length $\rho \sim u$ by $\rho := \Delta(0)/|\Delta'(0^+)|$; this allows one to define the dimensionless quantity $\mathcal{A}$ in Eq. (81). As a consequence, if the qKPZ equation is the effective field theory in the limit of $m \to 0$, then the ratio $\mathcal{A}$ needs to converge to the universal limit set by the qKPZ field theory. That this is indeed the case can be seen on Fig. 15. In the two models simulated, the amplitude ratio converges to the same value,

$$\mathcal{A}^{d=1} = 1.10(2). \tag{83}$$

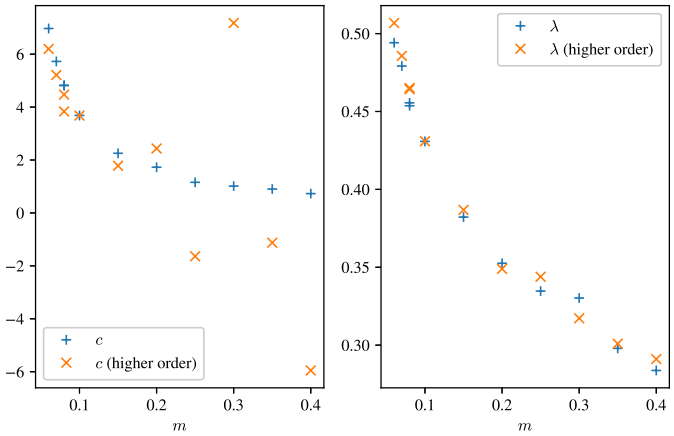

FIG. 17. Comparison of the different formula (Eq. (78) and Eq. (B2) for a formula based on fits to higher order harmonics) for determining c and λ, for aDep in $d = 1$. We can see that there is good agreement for λ but for c the higher order harmonics are too noisy for $m \geq 0.2$ to determined c with a good precision.

VI. CONCLUSION

We showed through theoretical arguments and numerical tests that anharmonic depinning, qKPZ, and the cellular automaton TL92 are in the same universality class, the qKPZ universality class, for $d \leq 2$. For $2 < d \leq 4$, there is evidence that TL92 departs from the qKPZ universality class (which still includes anharmonic depinning at those dimensions). We then elucidated the scaling relations for driving through a parabolic confining potential. This allowed us to understand statics and dynamics of our system. Finally, we developed an algorithm to measure the renormalized (effective) coefficients of the continuity equation. Our work will be useful to constrain, and ultimately construct the field theory presented in a sequel to this work [50].

We believe that our technique to extract the effective coupling constants by measuring the static response of the system under spatially modulated perturbations may yield important information in other systems that lack a proper field theoretic description. As an example, we started to extend it to the KPZ equation itself.

ACKNOWLEDGMENTS

We thank Alberto Rosso for useful discussions. JAB acknowledges support from NSF grant DMS-2052616. MAM acknowledges financial support from the Spanish Ministry and Agencia Estatal de investigación (AEI) through Project of I+D+i Ref. PID2020-113681GB-I00, financed by MICIN/AEI/10.13039/501100011033 and FEDER "A way to make Europe".

Appendix A: Why $z \neq 1$

In Ref. [5] the authors provide a heuristic argument for $z = 1$ in $d = 1$, while for higher dimension they conjecture that $z = d_{\min}$ with $d_{\min}$ the exponent on how the shortest-path length on a d dimensional critical percolating cluster scales with the Euclidean distance. Our simulations invalidate this heuristics. Here we give theoretical arguments as to why this heuristics fails. Ref. [5] studies TL92 with parallel updates. After an avalanche, they define the path of invaded cells as the path (in $1d$) from the cell from which it was invaded to the cell it invaded. Then they assert that the path length from the start of the avalanche to site i is equal to the time it took for cell i to be invaded. Then z is defined by $T \propto \ell^z$ with T the avalanche duration and ℓ the lateral extension of the avalanche. Since $\xi_\perp/\xi_m \to 0$, the invading path is considered rough as the path along the blocking configuration, so $\ell \approx \xi_m$. As a result they find $z = 1$. However, equating the length of the invading path with the duration of an avalanche is problematic: After reaching site i, the avalanche can change direction and then come back, and as a result the duration is under estimated, and $z > 1$.

In higher dimensions, this under-estimation persists, but is associated with another problem, that over-estimates z: since $\xi_\perp/\xi_m \to 0$ they model the $d+1$ dimensional space in which the invading path lives as a d dimensional critical percolation cluster, and then declare the invading path to be the shortest distance between two points on this percolation cluster. However, the transport properties of percolation clusters are highly dependent on the proportion of singly connected cells [61] (i.e. cells that if removed separate the percolation cluster in two). The existence of another dimension through which the path can go changes the statistics of those singly-connected cells. There are far more ways to reach one target, and as a result the time it takes to reach it may be smaller and z over-estimated.

Appendix B: Details of the algorithm

1. Numerical details

In Fig. 16 we show the results of measuring the modes of the interface for different amplitudes of the driving. One has to be careful to be in the small-perturbation limit. We find that taking the maximum perturbation amplitude to be $A = \frac{L}{40}$ to be appropriate. The number of points needed within that range to have a good precision on the polynomial fit is hard to deduce in advance, and varies with m. We find that sometimes the small perturbation limit is reached before $A = \frac{L}{40}$ and in that case it is good to have more points in order to maintain a good fit for the polynomials. A good rule of thumb is to have around 50 points.

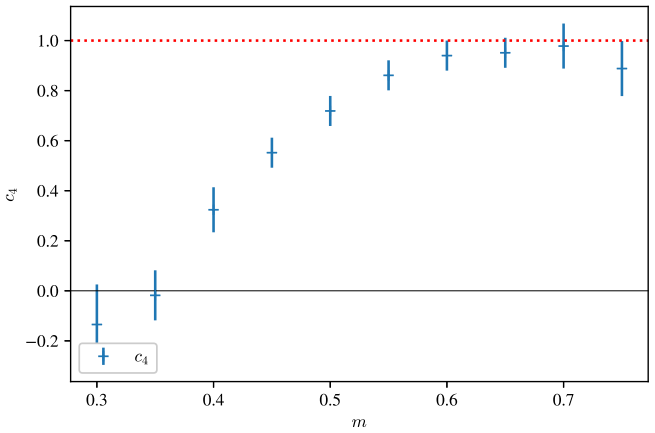

FIG. 18. Effective anharmonicity c_4 determined for anharmonic depinning using Eq. (B3). $L = 64$ and the initial condition is $c_4 = 1$ (red dotted line). The measured effective c_4 decreases as m decreases, vanishing within the precision of our simulation when $m \approx 0.3$. There the error for c_4 increases, as the small system sees more system-spanning avalanches, crossing over to a single-particle behavior. Increasing L further increases this error, since c_4 is determined through a high-order harmonics of the driving signal, and scales $\sim L^4$ appearing in Eq. (B3). Still, qualitatively this confirms that c_4 can be dropped in the effective long-distance description of the model.

2. Higher-order relations

There are higher order relations for λ and c. Here we put them, for completeness.

$$c(m) = \left(\frac{^2u_0}{^2u_2} - 1\right)\frac{m^2\ell^2}{4}, \tag{B1}$$

$$\lambda(m) = \frac{4\ell^2}{m^4}\left(m^2 + \frac{4c}{\ell^2}\right)\left(m^2 + \frac{c}{\ell^2}\right)^2\, ^2u_2. \tag{B2}$$

In Fig. 17 we can see that for smaller m, the higher order formulas agrees with their lower order counterpart. For higher m the signal for c determined with Eq. (B2) is too noisy. For λ there is good agreement for all m.

3. Crossover and higher-order anharmonic terms

An interesting question is the crossover from the microscopic model, e.g. in anharmonic depinning which contains a coefficient c_4. How does this terms decrease with m? To

answer these questions, we derive a formula for the expression of c_4. If a c_4 term is present, then the lowest order in A is A^3. We find that there is a contribution of c_4 on the first mode, written for compactness in terms of ${}^j u_i$, λ and c,

$$c_4(m) = -4\frac{\ell^4}{({}^1u_1)^3}\left[\frac{\lambda {}^1u_1{}^2 u_2}{\ell^2} + {}^3u_1\left(m^2 + \frac{c}{\ell^2}\right)\right]. \quad \text{(B3)}$$

c_4 appears as a third-order perturbation in A. Since it comes from higher harmonics, it is more heavily suppressed as the system becomes larger. As a result, small system sizes (and large m) must be considered to measure accurately c_4. However, there is a tradeoff, since c_2 and λ are determined with a lesser accuracy for smaller systems size. The result for an initial anharmonic depinning equation with $c_4 = 1$ are presented in Fig. 18. We see that at large m the microscopic value $c_4 = 1$ is obtained. Reducing m to about 0.35, the effective c_4 becomes too small to be distinguishable from the noise.

[1] T. Giamarchi and P. Le Doussal, *Elastic theory of flux lattices in the presence of weak disorder*, Phys. Rev. B **52** (1995) 1242–70, cond-mat/9501087.

[2] J.A. Bonachela, C.D. Nadell, J.B. Xavier and S.A. Levin, *Universality in bacterial colonies*, J. Stat. Phys. **144** (2011) 303–315.

[3] M.A.C. Huergo, N.E. Muzzio, M.A. Pasquale, P.H.Pedro González, A.E. Bolzán and A.J. Arvia, *Dynamic scaling analysis of two-dimensional cell colony fronts in a gel medium: A biological system approaching a quenched Kardar-Parisi-Zhang universality*, Phys. Rev. E **90** (2014) 022706.

[4] M. Alava and M.A. Muñoz, *Interface depinning versus absorbing-state phase transitions*, Phys. Rev. E **65** (2002) 026145.

[5] L.A.N. Amaral, A.-L. Barabási, S.V. Buldyrev, S.T. Harrington, S. Havlin, R. Sadr-Lahijany and H.E. Stanley, *Avalanches and the directed percolation depinning model: Experiments, simulations, and theory*, Phys. Rev. E **51** (1995) 4655–4673.

[6] R. Planet, L. Díaz-Piola and J. Ortín, *Capillary jumps of fluid-fluid fronts across an elementary constriction in a model open fracture*, Phys. Rev. Fluids **5** (2020) 044002.

[7] R. Holtzman, M. Dentz, R. Planet and J. Ortín, *The origin of hysteresis and memory of two-phase flow in disordered media*, Communications Physics **3** (2020) 222.

[8] K.J. Wiese, *Theory and experiments for disordered elastic manifolds, depinning, avalanches, and sandpiles*, ROPP **accepted** (2021), arXiv:2102.01215.

[9] H. Hinrichsen, *Non-equilibrium critical phenomena and phase transitions into absorbing states*, Adv. Phys. **49** (2000) 815–958, cond-mat/0001070.

[10] D.S. Fisher, *Interface fluctuations in disordered systems:* $5-\varepsilon$ *expansion*, Phys. Rev. Lett. **56** (1986) 1964–97.

[11] O. Narayan and D.S. Fisher, *Threshold critical dynamics of driven interfaces in random media*, Phys. Rev. B **48** (1993) 7030–42.

[12] T. Nattermann, S. Stepanow, L.-H. Tang and H. Leschhorn, *Dynamics of interface depinning in a disordered medium*, J. Phys. II (France) **2** (1992) 1483–8.

[13] H. Leschhorn, T. Nattermann, S. Stepanow and L.-H. Tang, *Driven interface depinning in a disordered medium*, Annalen der Physik **509** (1997) 1–34, arXiv:cond-mat/9603114.

[14] P. Chauve, P. Le Doussal and K.J. Wiese, *Renormalization of pinned elastic systems: How does it work beyond one loop?*, Phys. Rev. Lett. **86** (2001) 1785–1788, cond-mat/0006056.

[15] P. Le Doussal, K.J. Wiese and P. Chauve, *2-loop functional renormalization group analysis of the depinning transition*, Phys. Rev. B **66** (2002) 174201, cond-mat/0205108.

[16] P. Le Doussal, K.J. Wiese and P. Chauve, *Functional renormalization group and the field theory of disordered elastic systems*, Phys. Rev. E **69** (2004) 026112, cond-mat/0304614.

[17] J.P. Sethna, K.A. Dahmen and C.R. Myers, *Crackling noise*, Nature **410** (2001) 242–250.

[18] A. Rosso, P. Le Doussal and K.J. Wiese, *Avalanche-size distribution at the depinning transition: A numerical test of the theory*, Phys. Rev. B **80** (2009) 144204, arXiv:0904.1123.

[19] P. Le Doussal and K.J. Wiese, *Size distributions of shocks and static avalanches from the functional renormalization group*, Phys. Rev. E **79** (2009) 051106, arXiv:0812.1893.

[20] P. Le Doussal, A.A. Middleton and K.J. Wiese, *Statistics of static avalanches in a random pinning landscape*, Phys. Rev. E **79** (2009) 050101 (R), arXiv:0803.1142.

[21] P. Le Doussal, M. Müller and K.J. Wiese, *Avalanches in mean-field models and the Barkhausen noise in spin-glasses*, EPL **91** (2010) 57004, arXiv:1007.2069.

[22] P. Le Doussal and K.J. Wiese, *Elasticity of a contact-line and avalanche-size distribution at depinning*, Phys. Rev. E **82** (2010) 011108, arXiv:0908.4001.

[23] P. Le Doussal and K.J. Wiese, *First-principle derivation of static avalanche-size distribution*, Phys. Rev. E **85** (2011) 061102, arXiv:1111.3172.

[24] P. Le Doussal, M. Müller and K.J. Wiese, *Equilibrium avalanches in spin glasses*, Phys. Rev. B **85** (2012) 214402, arXiv:1110.2011.

[25] P. Le Doussal and K.J. Wiese, *Avalanche dynamics of elastic interfaces*, Phys. Rev. E **88** (2013) 022106, arXiv:1302.4316.

[26] A. Dobrinevski, P. Le Doussal and K.J. Wiese, *Statistics of avalanches with relaxation and Barkhausen noise: A solvable model*, Phys. Rev. E **88** (2013) 032106, arXiv:1304.7219.

[27] A. Dobrinevski, P. Le Doussal and K.J. Wiese, *Avalanche shape and exponents beyond mean-field theory*, EPL **108** (2014) 66002, arXiv:1407.7353.

[28] T. Thiery, P. Le Doussal and K.J. Wiese, *Spatial shape of avalanches in the Brownian force model*, J. Stat. Mech. **2015** (2015) P08019, arXiv:1504.05342.

[29] L.E. Aragon, A.B. Kolton, P. Le Doussal, K.J. Wiese and E. Jagla, *Avalanches in tip-driven interfaces in random media*, EPL **113** (2016) 10002, arXiv:1510.06795.

[30] M. Delorme, P. Le Doussal and K.J. Wiese, *Distribution of joint local and total size and of extension for avalanches in the Brownian force model*, Phys. Rev. E **93** (2016) 052142, arXiv:1601.04940.

[31] G. Durin, F. Bohn, M.A. Correa, R.L. Sommer, P. Le Doussal and K.J. Wiese, *Quantitative scaling of magnetic avalanches*, Phys. Rev. Lett. **117** (2016) 087201, arXiv:1601.01331.

[32] T. Thiery, P. Le Doussal and K.J. Wiese, *Universal correlations between shocks in the ground state of elastic interfaces in disordered media*, Phys. Rev. E **94** (2016) 012110, arXiv:1604.05556.

[33] Z. Zhu and K.J. Wiese, *The spatial shape of avalanches*, Phys. Rev. E **96** (2017) 062116, arXiv:1708.01078.

[34] J.A. Bonachela, M. Alava and M.A. Muñoz, *Cusps in systems with (many) absorbing states*, Phys. Rev. E **79** (2009) 050106(R), arXiv:0810.4395.

[35] P. Le Doussal and K.J. Wiese, *How to measure Functional RG fixed-point functions for dynamics and at depinning*, EPL **77** (2007) 66001, cond-mat/0610525.

[36] A.A. Middleton, P. Le Doussal and K.J. Wiese, *Measuring functional renormalization group fixed-point functions for pinned manifolds*, Phys. Rev. Lett. **98** (2007) 155701, cond-mat/0606160.

[37] P. Le Doussal, K.J. Wiese, S. Moulinet and E. Rolley, *Height fluctuations of a contact line: A direct measurement of the renormalized disorder correlator*, EPL **87** (2009) 56001, arXiv:0904.4156.

[38] K.J. Wiese, M. Bercy, L. Melkonyan and T. Bizebard, *Universal force correlations in an RNA-DNA unzipping experiment*, Phys. Rev. Research **2** (2020) 043385, arXiv:1909.01319.

[39] C. ter Burg, F. Bohn, F. Durin, R.L. Sommer and K.J. Wiese, *Force correlations in disordered magnets*, (2021), arXiv:2109.01197.

[40] L.-H. Tang and H. Leschhorn, *Pinning by directed percolation*, Phys. Rev. A **45** (1992) R8309–12.

[41] S.V. Buldyrev, A.-L. Barabasi, F. Caserta, S. Havlin, H.E. Stanley and T. Vicsek, *Anomalous interface roughening in porous media: experiment and model*, Phys. Rev. A **45** (1992) R8313–16.

[42] S.V. Buldyrev, S. Havlin and H.E. Stanley, *Anisotropic percolation and the d-dimensional surface roughening problem*, Physica **A 200** (1993) 200–211.

[43] M. Kardar, G. Parisi and Y.-C. Zhang, *Dynamic scaling of growing interfaces*, Phys. Rev. Lett. **56** (1986) 889–892.

[44] S. Atis, A.K. Dubey, D. Salin, L. Talon, P. Le Doussal and K.J. Wiese, *Experimental evidence for three universality classes for reaction fronts in disordered flows*, Phys. Rev. Lett. **114** (2015) 234502, arXiv:1410.1097.

[45] T. Chevalier, A. K. Dubey, S. Atis, A. Rosso, D. Salin and L. Talon, *Avalanches dynamics in reaction fronts in disordered flows*, Phys. Rev. E **95** (2017) 042210.

[46] A. Rosso, A.K. Hartmann and W. Krauth, *Depinning of elastic manifolds*, Phys. Rev. E **67** (2003) 021602, cond-mat/0207288.

[47] L.-H. Tang, M. Kardar and D. Dhar, *Driven depinning in anisotropic media*, Phys. Rev. Lett. **74** (1995) 920–3.

[48] P. Le Doussal and K.J. Wiese, *Functional renormalization group for anisotropic depinning and relation to branching processes*, Phys. Rev. E **67** (2003) 016121, cond-mat/0208204.

[49] I. Jensen, *Critical behavior of the pair contact process*, Phys. Rev. Lett. **70** (1993) 1465–1468.

[50] G. Mukerjee and K.J. Wiese, *Depinning in the quenched Kardar-Parisi-Zhang class II: Field theory*, unpublished (2022).

[51] K. Sneppen, *Self-organized pinning and interface growth in a random medium*, Phys. Rev. Lett. **69** (1992) 3539–3542.

[52] Belén Moglia, E.V. Albano, P. Villegas and M.A. Muñoz, *Interfacial depinning transitions in disordered media: revisiting an old puzzle*, J. Stat. Mech. **2014** (2014) P10024.

[53] C. Lee and J.M. Kim, *Depinning transition of the quenched Kardar-Parisi-Zhang equation*, J. Korean Phys. Soc. **47** (2005) 13–17.

[54] A.A. Middleton, *Asymptotic uniqueness of the sliding state for charge-density waves*, Phys. Rev. Lett. **68** (1992) 670–673.

[55] A. Rosso and W. Krauth, *Origin of the roughness exponent in elastic strings at the depinning threshold*, Phys. Rev. Lett. **87** (2001) 187002, cond-mat/0104198.

[56] N. Araújo, P. Grassberger, B. Kahng, K. J. Schrenk and R. M. Ziff, *Recent advances and open challenges in percolation*, Eur. Phys. J. Spec. Top. **223** (2014) 2307–2321, arXiv:1404.5325.

[57] D. Dhar, *Directed percolation and directed animals*, (2017), arXiv:1703.07541.

[58] A.-L. Barabasi, G. Grinstein and M.A. Muñoz, *Directed surfaces in disordered media*, Phys. Rev. Lett. **76** (1996) 1481–4.

[59] E.E. Ferrero, S. Bustingorry and A.B. Kolton, *Non-steady relaxation and critical exponents at the depinning transition*, Phys. Rev. E **87** (2013) 032122, arXiv:1211.7275.

[60] P. Grassberger, D. Dhar and P. K. Mohanty, *Oslo model, hyperuniformity, and the quenched Edwards-Wilkinson model*, Phys. Rev. E **94** (2016) 042314, arXiv:1606.02553.

[61] D. Stauffer and A.A. Aharony, *An Introduction to Percolation Theory*, Taylor & Francis, 1994.

[62] Y.-J. Chen, S. Papanikolaou, J.P. Sethna, S. Zapperi and G. Durin, *Avalanche spatial structure and multivariable scaling functions: Sizes, heights, widths, and views through windows*, Phys. Rev. E **84** (2011) 061103.

[63] A. Rosso and W. Krauth, *Monte Carlo dynamics of driven strings in disordered media*, Phys. Rev. B **65** (2001) 012202, cond-mat/0102017.

CONTENTS